



# Selection of backfill grout for shallow geothermal systems: Materials investigation and thermo-physical analysis

Ludovico Mascarin<sup>a</sup>, Enrico Garbin<sup>b,\*</sup>, Eloisa Di Sipio<sup>a</sup>, Giorgia Dalla Santa<sup>a</sup>, David Bertermann<sup>c</sup>, Gilberto Artioli<sup>a</sup>, Adriana Bernardi<sup>d</sup>, Antonio Galgaro<sup>a</sup>

<sup>a</sup> University of Padova, Department of Geosciences, Via Gradenigo 6, 35131 Padova, Italy

<sup>b</sup> University of Padova, Inter-Departmental Research Centre for the Study of Cement Materials and Hydraulic Binders (CIRCe Centre), Via G. Gradenigo 6, 35131 Padova, Italy

<sup>c</sup> GeoZentrum Nordbayern, Friedrich-Alexander University Erlangen-Nuremberg, Department of Geology, Schlossgarten 5, 91054 Erlangen, Germany

<sup>d</sup> National Research Council of Italy (CNR), Institute of Atmospheric Sciences and Climate (ISAC), Corso Stati Uniti 4, 35127 Padova, Italy

## ARTICLE INFO

### Keywords:

Shallow geothermal systems  
Backfill grouts  
Borehole heat exchangers  
Thermo-physical properties  
Grout flowability

## ABSTRACT

A main aspect of the geothermal well design is the selection of grouts backfilling the space between a geothermal probe and the surrounding ground, taking into consideration the mineralogical, thermo-physical, mechanical and flowability properties. The EU GEO4CIVHIC project aimed at developing efficient and cost-effective geothermal systems suitable for the air-conditioning refurbishment of urban buildings. A selection of different grouts was performed to ensure the whole efficiency of shallow geothermal heat exchangers designed within the project. Experimental tests were executed to identify flowable grouts with the best possible combination of different material properties, while also fulfilling a competitive cost target set forth in the preliminary project cost analysis. Grout acceptance criteria were defined: a working time of at least 4 h, a water bleeding target of 2% and a volumetric shrinkage upper bound of 4%, a thermal conductivity in water saturated conditions of at least  $1.4$  to  $1.5 \text{ Wm}^{-1}\text{K}^{-1}$ , a compressive strength range of  $1$  to  $2.1 \text{ MPa}$ , a flow time range of  $60 \pm 15 \text{ s}$ . Two out of six commercial grouts were selected for installations onsite.

## 1. Introduction

Grouts formulated for geothermal energy applications should comply with practical installation requirements and durability performance of borehole heat exchangers. Conversely, the research devoted to geothermal grouts mainly focused on improving thermal conductivity by adding fillers or admixtures, testing suitable hydraulic and mechanical properties, comparing different kind of grouts [1,2,3]. The novelty of this paper consists in presenting a multi-criteria analysis of commercial geothermal grouts, providing a definition of quantitative acceptability ranges for each thermo-physical property investigated as well as a cost target. The paper presents a holistic approach to identify the main requirements for a commercial geothermal grout useful for the installation of coaxial heat exchangers.

Nowadays, shallow geothermal heat exchange is widely acknowledged as a cost-effective means of providing building space heating and

cooling, and thus potentially utilizing electricity or primary fuels more efficiently than conventional air-conditioning systems [4]. The heat or cold stored in surface water, groundwater aquifers and ground soil/rock can be exploited directly or by using heat pumps coupled with heat exchangers. Two main categories of ground source heat pumps (GSHPs) are commonly adopted, the open-loop or closed-loop systems. The first uses groundwater, the second uses water or a mixture of water and additives (e.g., antifreeze) as a heat transfer medium [5]. The performance of low enthalpy geothermal systems (usually up to 200 m depth) depends directly on local conditions such as the ground thermal properties [6]. Nonetheless, these systems are currently a remarkably interesting option for energetic refurbishment of existing and historical buildings thanks to the latest technological improvements of GSHPs for heating/cooling purposes and domestic hot water production [7]. In fact, GSHPs ensure clean energy production according to the European Union 2009/28/CE directive and are appealing because of their low

\* Corresponding author.

E-mail addresses: [ludovico.mascarin@phd.unipd.it](mailto:ludovico.mascarin@phd.unipd.it) (L. Mascarin), [enrico.garbin@dicea.unipd.it](mailto:enrico.garbin@dicea.unipd.it) (E. Garbin), [eloisa.disipio@unipd.it](mailto:eloisa.disipio@unipd.it) (E. Di Sipio), [giorgia.dallasanta@unipd.it](mailto:giorgia.dallasanta@unipd.it) (G. Dalla Santa), [david.bertermann@fau.de](mailto:david.bertermann@fau.de) (D. Bertermann), [gilberto.artioli@unipd.it](mailto:gilberto.artioli@unipd.it) (G. Artioli), [a.bernardi@isac.cnr.it](mailto:a.bernardi@isac.cnr.it) (A. Bernardi), [antonio.galgaro@unipd.it](mailto:antonio.galgaro@unipd.it) (A. Galgaro).

<https://doi.org/10.1016/j.conbuildmat.2021.125832>

Received 20 May 2021; Received in revised form 22 November 2021; Accepted 23 November 2021

Available online 13 December 2021

0950-0618/© 2021 The Authors.

Published by Elsevier Ltd.

This is an open access article under the CC BY-NC-ND license

(<http://creativecommons.org/licenses/by-nc-nd/4.0/>).

energy consumption and independence of supply [8]. GSHPs consist mainly of three parts: a heat pump, borehole heat exchangers (BHEs) installed vertically or horizontally in the ground and a heat transfer medium circulating in the BHEs [9,10,11,12]. The main task of a BHEs is to facilitate the heat exchange from the ground to the fluid inside the pipes and vice versa with as little thermal resistance as possible. Several factors influence the heat exchange: pipe material, wall thickness, pipe surface properties, fluid flow velocity, BHE geometry, borehole diameter, grouting, thermal properties of the ground. For BHEs, all geometries can be grouped into two basic patterns, U-tube and coaxial pipes. The main difference is that U-tube always show a mirror-symmetry (generally single or double U-pipes), while coaxial BHE are radially symmetric (simple coaxial, complex coaxial and helicoidal). The most common worldwide BHEs vertical technology consists of U-tube pipes (diameter 20–40 mm) made mainly of High-Density Polyethylene (HDPE) backfilled into boreholes of 20–200 m depth and 100 mm to 200 mm diameter wide. Less common are HDPE or stainless-steel coaxial pipe inserted in a grouted borehole [13,14,15]. HDPE tends to be used in modern systems instead of polyethylene (PE) or metallic solutions due to its robustness, resistance to corrosion and affordability, while currently new materials are tested to improve the overall efficiency of the pipes [14].

The focus of this paper is on coaxial heat exchangers, with the inner and outer pipes made of stainless steel (Fig. 1). According to EU GEO4CIVHIC and Cheap GSHPs projects [16,17], this setup can allow higher thermal exchange over the use of single U-pipe configuration, thus delivering an economically favourable minimization of the borehole length [18–19]. In fact, the configuration with coaxial pipes provides better thermal performance over time due to the higher thermal capacitance of the heat-carrier fluid and the lower borehole thermal resistance [18]. Flowable grouts, backfilling the space between the pipe and the surrounding ground, are part of the installation process of all vertical BHEs [20,21]. Grouts are fundamental for promoting an efficient thermal coupling between the borehole wall lithology and the heat exchanger, the borehole stability, the zonal sealing of the wellbore to counteract technical fluids leakage and to prevent connection among aquifers, while preserving the surrounding environment since they are chemically inert [20,21,22]. The annular space in the borehole is usually backfilled with (i) conventional grouts made of bentonite clay, binary soil mixtures and/or cement, (ii) thermally enhanced blends improved with mineral additives and fine aggregate, (iii) modern mixtures as Controlled Low-Strength Material (CLSM) and Phase Change Materials (PCMs) as stand-alone or mixed with grout [23,24,25,26,27,28]. A good heat transfer between BHE and the surrounding ground contributes to reduce the borehole thermal resistance, also affected by the interplay between probe geometry, borehole diameter, grout thickness, heat

transfer fluid type and flow rate within the probe. In addition, the fluctuating temperature in proximity to the pipes, induced by short and rapid unbalanced fluctuations in thermal loads, reduces GSHP efficiency. This is because the rapid ground temperature changes, due to the combined effect of ground thermal conductivity and specific heat, also affect the heat transfer fluid temperature within the BHE. Therefore, abating this temperature fluctuation by using grouts leads to a better heat transfer and to a reduction of the total BHE length needed, with a consequent economic advantage due to lower installation costs [27,28]. However, according to the Scandinavian practice, especially adopted in Sweden, the space between the probe and the borehole's walls may be filled with groundwater, due to the good quality of the bedrock, where the local water table is near the surface and the overall hydrogeological conditions permit it [15,28].

High-efficiency systems use grouts with a thermal conductivity usually equal to that of the surrounding geological formations and with a low air voids fraction, which can reduce the thermal interference between the outer coaxial pipe and the underground enhancing the heat transfer rates [29,30]. Thermally enhanced grouts with conductivity between 1,7 and 2,1  $\text{Wm}^{-1}\text{K}^{-1}$  can allow a larger heat transfer with the geological surrounding if necessary [30,31,32]. The addition of fine silica sand or graphite are typical enhancers of the thermal properties [31,33,34]. Onsite heat-exchangers installations should be performed with grouts provided with adequate pumpability, viscosity and mechanical strength to thoroughly backfill the annulus between the probe and the underground without any gap, to guarantee the aquifers' isolation and to stabilise the borehole, while avoiding mechanical failures due to thermal cycles [20,22,29,34,35,36]. Generally, different techniques for grouting of the empty annulus are available [37,38]. Nonetheless, the injection of the grout from the bottom appears to be the most appropriate for shallow geothermal systems [37,38]. Moreover, to prevent the leakage of contaminated surface water downhole, or inter-aquifer connection, the grouts should have a hydraulic conductivity of  $< 10^{-9}$  m/s, as suggested by the UK Environmental Agency [39].

Therefore, a dedicated investigation was devoted to the identification of most appropriate grouts having optimal thermo-physical properties thus, ensuring a performing installation and energetic operability of the coaxial heat exchangers designed in the GEO4CIVHIC project [16].

A careful selection of commercial grouts suitable for shallow geothermal systems (Fig. 1) was carried out. The mineralogical composition, heat of hydration, density, volumetric stability, thermal conductivity, compressive strength, flowability and pumpability were investigated and analysed in order to select efficient grouts. The selection was based on acceptance criteria developed during the experimental work, and a competitive cost target set forth in a preliminary cost

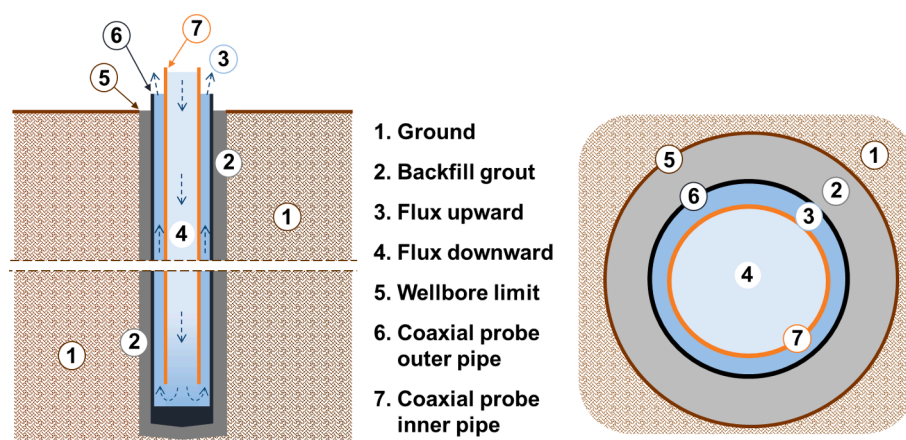


Fig. 1. Sealing of the coaxial geothermal heat exchangers by filling the annular space between the probe and the geological formations exposed by the wellbore: side view (left) and top view (right).

analysis [40]. Two grouts, out of six commercial products, were chosen because of their balanced trade-off of different thermo-physical properties, which delivered a promising thermal coupling of the probe with the underground.

## 2. Materials and methods

### 2.1. Selection of grouts and testing methods

The initial general pre-requisites for the grout backfilling the annular gap were: (a) a preferred working time of 4 h, which was the maximum allowed time spanning from grout mixing to complete BHE installation (during this time the grout should remain flowable and should not set); (b) a density of the fresh grout after mixing smaller than the gross apparent density of the coaxial probe; (c) a product volumetrically stable, thus having no or limited volumetric shrinkage and no or limited segregation and water bleeding; (d) a product with an adequate thermal conductivity for ensuring the largest probe-soil heat exchange; (e) a backfill material with a sufficient compressive strength, possibly larger than 1 MPa, in moist conditions and with adequate deformability to avoid stress concentrations over the casing length and cracking due to cyclic thermal loads; (f) a grout sufficiently fluid to be easily pumped and able to fill an annulus about 100 m long, while having an adequate yield stress for tolerating the probable presence of groundwater; (g) a product with a retail cost smaller than 0.45 €/kg, as per the 2020 available price lists [40].

Six commercial grouts suitable for backfilling cavities, named BF, MP, RF, FSB, HBG and LS, were chosen from the Italian construction market to test the behaviour of three different types of blends: cement-free pozzolanic grouts (BF, MP), cement grouts (RF, FSB), cement pozzolanic/clayey grouts (HBG, LS). In general, the datasheets declared: few times a working time larger than 5 h, a density of the fresh grout below 1900 kg/m<sup>3</sup>, few times the absence of bleeding, most of the times a thermal conductivity larger than 1.5 Wm<sup>-1</sup>K<sup>-1</sup> and enhanced for geothermal purposes, most of the times a compressive strength after 28 days larger than 2.0 MPa. The datasheets also indicated the use of mineral or organic admixtures to ensure adequate flowability, and stressed the sealing capacity, which correlates with a low-enough permeability, of the products.

The six grouts were laboratory tested for: (i) mineralogical composition, (ii) calorimetric behaviour for monitoring the degree of hydration, (iii) density and volumetric stability via volumetric shrinkage and bleeding evaluation, (iv) thermal conductivity, (v) compressive strength, (vi) flowability and rheological properties for evaluating the pumpability and possibly assessing the tolerance to groundwater presence (washout resistance). These measurements of grout parameters are in line with those indicated in the EN 12715 [41].

### 2.2. XRD measurements

X-ray diffraction (XRD) was performed on milled powdered samples mixed with 10 wt% zinc oxide internal standard to determine the amorphous fraction. The powders were measured with an X'Pert Pro diffractometer (Malvern-PANalytical) equipped with a Co-anode X-ray source and an X'Celerator detector. The diffraction patterns were gathered in the 3-85° 2θ region, with a 0.017° 2θ virtual step size, counting an equivalent time of 100 s per step. The XRD laboratory was at a temperature (T) of 20 ± 1 °C and relative humidity (RH) of 50%. The Rietveld quantitative phase analysis [42] was performed with Topas software [43].

### 2.3. Grouts mixing

Hydrated grouts were prepared with the water-to-solid ratios (w/s) recommended in the datasheets and by stirring the mixtures with an IKA mixer in two steps of about 1.5 min with an intermediate interval of

about 1 min. The mixing sequence was derived from that of EN 196-1 [44]. The rotation speed of the blade was progressively increased up to 385 rpm to allow a smooth and complete mixing of grout powder and water. Afterwards, grouts were manually re-mixed with a rubber spatula to check the absence of clumps and ensure the homogeneity of the material. The mixing was executed in laboratory conditions at T = 20 ± 2 °C and RH = 65%. Fresh state grouts were casted in the specific containers, moulds or apparatus necessary for each test.

### 2.4. Calorimetric measurements

Semi-adiabatic calorimetry was performed to draw hydration curves according to the RILEM Technical Committee 119-TCE [45]. Fresh grouts were poured into thermally insulating vessels, and the temperature variations of the mixtures were monitored with thermocouples.

### 2.5. Densities and volumetric stability measurements

The bulk density of the fresh fluid grouts was measured according to EN 1015-6 [46]. The apparent densities at the hardened state in moist and dry conditions were measured according to EN 1015-10 [47]. The moist density is related to samples that after demoulding were not oven dried but dipped in water and then stored in damp conditions within airtight boxes (T = 25 ± 2 °C, RH = 95%). In moist condition the apparent mass included the unbound water within the pore network. The volumetric stability of the grouts was evaluated after 56 days of curing by measuring the volumetric shrinkage of three specimens, which were casted on 5 × 5 × 5 cm<sup>3</sup> moulds [48]. The volumetric shrinkage values were compared versus acceptable linear shrinkage values for flowable Controlled Low Strength Materials (CLSM) as indicated by ACI 229R-13 [49]. Noteworthy, CLSM are self-compacted, flowable, plastic soil-cement mixtures used primarily as a backfill for trenches or superficial excavations that in the last five years were successfully used as backfill for shallow geothermal systems [50,51].

### 2.6. Bleeding measurements

The stability of those grouts showing a marked volumetric shrinkage, and thus probably with segregation issues, was further controlled via bleeding tests according to ASTM C 940-16 [52].

The effect of the water content on the bleeding rate was investigated by lowering step-by-step the reference mixing water-to-solid ratio (w/s). The evolution of the bleed water was monitored during the first 120 min after mixing as performed in [51,53,54]. A graduated cylinder of 1000 ml and having a diameter of 60 mm was filled with 1 L of fresh grout [52]. The cylinder was covered to prevent evaporation.

### 2.7. Thermal conductivity measurements

The thermal conductivity was measured per each grout on the flat surfaces of three 5 × 5 × 5 cm<sup>3</sup> cubic specimens [48] adopting the optical scanning method (TCS-Thermal Conductivity Scanning by Lippmann) [55]. This method allows to measure the thermal properties of sample surface with a high precision non-contact device. A focused, mobile and continuously operated heat source works in combination with two infrared temperature sensors to determine the thermal properties profile of several samples, also taking into account the presence of inhomogeneity or anisotropies. The method is based on solutions of the thermal conduction equation for a quasi-stationary temperature field in a movable coordinate system. The bulk thermal conductivity results from the average of the values gathered along a scan line. Measurements of the thermal conductivity were repeated on three equal samples both in dry and water saturated conditions. At first, to obtain the so-called dry specimens, the samples were dried in a fan-forced oven at 70 °C for 24 h and then stored in an air-conditioned room (24 h, T = 22 ± 1 °C, RH = 30–50%) to reach the thermal equilibrium with the probe sensor. Any

change in effective porosity and mineral assemblage related to pore fabric alteration and hydration-water removal was thus avoided. Subsequently, to consider the onsite groundwater, the specimens were gradually water saturated by submersion at room temperature  $T = 20 \pm 5$  °C and constant pressure for 48. Then, the porosity ( $\Phi$ ) of each sample was determined by the Archimedes' Principle, after having measured the dry, buoyant and saturated mass of the sample [56].

## 2.8. Compression tests

The  $5 \times 5 \times 5$  cm<sup>3</sup> cubic specimens, used also for the volumetric stability, were tested in compression according to [48,49]. Three cubic specimens were tested per each grout. The specimens were cured in moist conditions at ambient temperature ( $T = 25 \pm 2$  °C, RH = 95%) for 56 days before the mechanical testing. This curing period was adopted due to the possible low strength and pozzolanic components of some grouts that would necessitate a longer curing than the typical 28 days [57,58]. The compressive tests were performed with universal testing machines Galdabini SUN25 and Galdabini SUN60 having an accuracy of 0.03% and with full scales of 25 kN and 600 kN, respectively. The Galdabini SUN60 was used for BF, MP and HBG grouts. The Galdabini SUN25 was used for RF, FSB and LS grouts.

## 2.9. Flowability and rheological properties

The flowability of the selected grouts was assessed by using the flow cone apparatus of EN 445 [59], as allowed by [41]. This apparatus has a specific funnel-like geometry and a draining nozzle with a length of 60 mm and an internal diameter of 10 mm [59]. The use of this specific apparatus for the evaluation of the viscous properties of cement pastes and grouts has been described in [45,46]. The EN 445 [59] flow cone was used for measuring the efflux time of 1 L of grout in laboratory conditions ( $T = 20 \pm 2$  °C, RH = 65%). Per each grout, the measure was executed after mixing and repeated at every hour of the desired 4-hour working time. The grout was kept remixed while waiting further testing as indicated by [59], thus possibly simulating the turbulent state representative of onsite mixing, pumping and injection. As reference, the larger the flow time, the lower the flowability and the larger the viscosity of the grout [60,61].

Other flow cone apparatuses with different geometries are available. For instance, the flow cone apparatus of ASTM C939/C939M-16a [62] is used for testing the flowability of CLSM mixtures [49] and it will be useful for discussing the flowability of our grouts. This last apparatus has a cone-like geometry and a draining nozzle with a length of 1.5 in. (38.1 mm) and an internal diameter of 0.5 in. (12.7 mm). A fixed amount of grout (e.g., 1 L) would flow through the ASTM C939/C939M-16a cone [62] more rapidly than the EN 445 cone [59].

The pumpability of the grouts was assessed in detail with a rheometer Anton Paar MCR92 operating in plate-plate geometry (lower plate diameter of 50 mm, upper plate diameter of 25 mm). The gap between the parallel plates, in which the fresh material was confined, was set to 2 mm for all experiments. Ascending and descending logarithmic shear rate ramps were used to measure flow curves. The data of the descending ramps was used to estimate the rheological parameters.

Two common Non-Newtonian models for cement-based materials were used for fitting the flow behaviour of the grouts: the Herschel-Bulkley and the Bingham models [63,64]. In particular, the more refined Herschel-Bulkley model [63] was originally used to simulate the flow of shear-thinning fluids as the drilling muds [65], while the simpler and more practical Bingham model is suggested by the EN 12,715 [41] for modelling geotechnical grouts. The Herschel-Bulkley and Bingham models are described by Equation (1) and Equation (2), respectively:

$$\tau = c + k \cdot \dot{\gamma}^n \quad (1)$$

$$\tau = \tau_0 + \mu_{app} \cdot \dot{\gamma} \quad (2)$$

where  $\tau$  is the shear stress (Pa),  $c$  is the cohesion (Pa),  $k$  is the consistency index (Pa·s),  $\dot{\gamma}$  is the shear rate (s<sup>-1</sup>), and  $n$  is the flow index (which spans from 0 to 1 for materials with a shear-thinning flow behaviour),  $\tau_0$  is the yield stress,  $\mu_{app}$  is the apparent plastic viscosity (Pa·s).

An example of the fitting with the Herschel-Bulkley and the Bingham models of the flow data is shown in Fig. 2 for the rheological behaviour of the RF grout just after mixing. In this case the Herschel-Bulkley model function provided a closer fit of the flow curve compared to the Bingham model, which is represented by the tangent to the second part of the curve. Nevertheless, the Bingham model was used to estimate the yield stress, which stands for the critical shear stress above which plastic deformations occur, and the apparent viscosity that can be related to the flow resistance.

## 3. Results and discussion

### 3.1. Mineralogical investigation

The XRD diffraction patterns of the selected grouts are shown in Fig. 3 and the corresponding quantitative phase analysis is reported in Table 1. All the products, aside from HBG, are characterized by a fraction of carbonates (calcite and/or dolomite) higher than 50% that reasonably act as inert fillers in grouting materials. The incorporation of calcitic or dolomitic siftings is aimed at improving the fresh-state stability (e.g. mitigation of bleeding and segregation, regulation of flowability) as observed for self-compacting blends [66,67,68,69].

Peaks associated to calcium hydroxide, or portlandite, were detected in pozzolanic grouts (BF, MP). These two materials presented a diffuse scattering hump particularly pronounced in the angular range between 30° and 40° 2 $\theta$ . This broad band may be reasonably associated to X-ray amorphous pozzolanic constituents. Likewise, the amorphous band appeared in the diffraction pattern of HBG. Moreover, this last material stood out for the peaks of graphite, which is occasionally added in geothermal grouts for improving the thermal conductivity [33,34].

Phyllosilicates were present in HBG and LS (Fig. 3). In particular, HBG was composed by an association of clay minerals such as illite, kaolinite and presumably the less common sepiolite as evidenced by the first low-angle peak ( $\sim 12.5$  Å) with broad shape. Illite is marked by the 002 peak at  $\sim 10$  Å ( $\sim 10^\circ$  2 $\theta$ ) and kaolinite by the 001 peak at  $\sim 7$  Å ( $\sim 14^\circ$  2 $\theta$ ). Kaolinite is referred to as 1:1 (or T-O) clay with reference to the layer stacking with tetrahedral and octahedral sheets. Instead, illite is distinguished by a 2:1 (or T-O-T) structure with stacked tetrahedral-octahedral-tetrahedral sequences and potassium ions to occupy the interlayer spacing. Sepiolite is a highly porous hydrated magnesium silicate with needle-like particles instead of plate-like particles as in illite and kaolinite. The XRD profile of LS was characterized by the presence

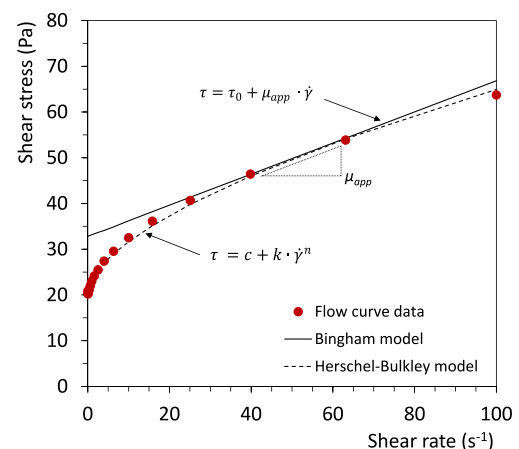
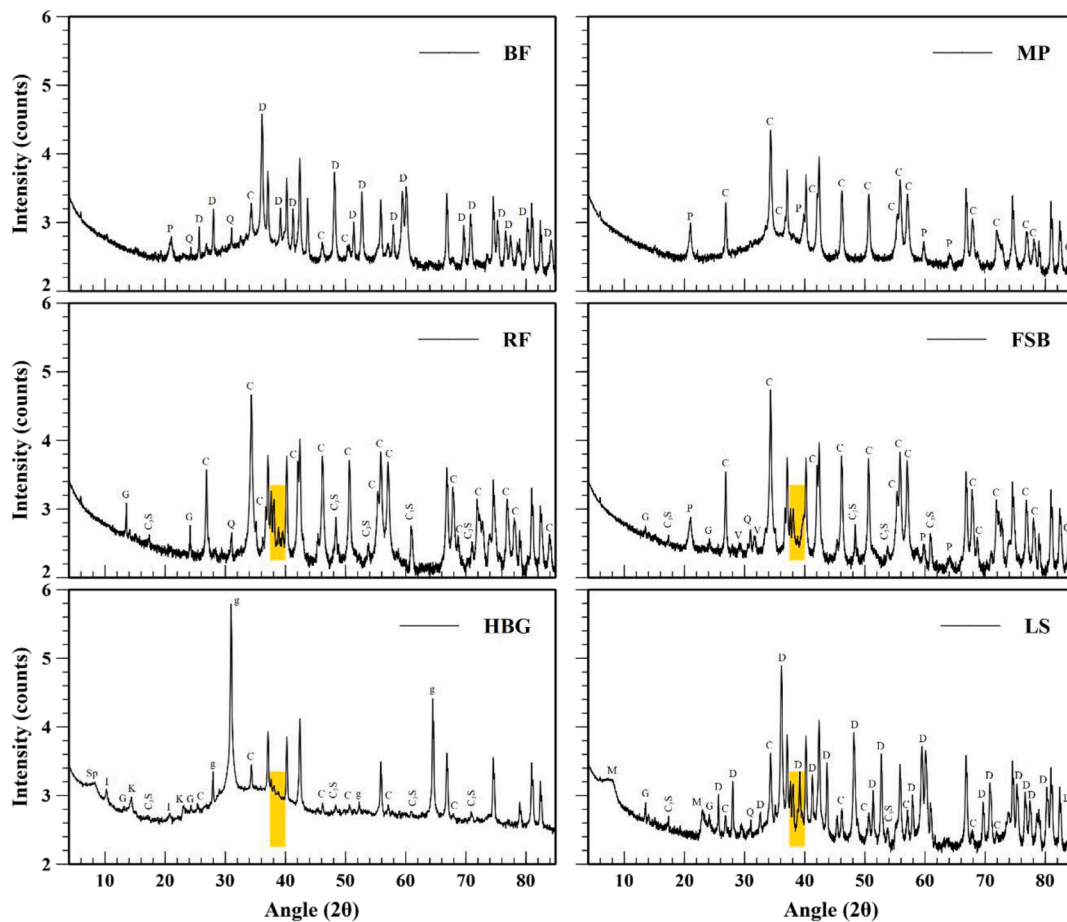


Fig. 2. Example of curve fitting for the Herschel-Bulkley and Bingham models.



**Fig. 3.** XRD diffraction patterns. Labels: C = calcite, D = dolomite, V = vaterite, Q = quartz, g = graphite, P = portlandite, G = gypsum, C<sub>3</sub>S = tricalcium silicate (the main cement clinker phase), I = illite, K = kaolinite, Sp = sepiolite, M = montmorillonite. The yellow frames highlight the diagnostic angular region for cement clinker phases. Not labelled peaks are associated to the ZnO internal standard. (For interpretation of the references to colour in this figure legend, the reader is referred to the web version of this article.)

**Table 1**

XRD quantitative phase analysis of raw materials. Composition in mass percentage (wt.%).

Mineral phases	BF	MP	RF	FSB	HBG	LS
Calcite	6.0	50.8	84.6	84.8	1.5	5.3
Dolomite	62.6	–	–	–	–	59.8
Vaterite	–	–	–	2.7	–	–
Portlandite	2.2	4.2	–	3.5	–	–
Quartz	0.8	–	0.5	0.6	–	0.1
Gypsum	–	–	0.6	0.3	0.2	0.9
Graphite	–	–	–	–	6.7	–
C <sub>3</sub> S/C <sub>2</sub> S	–	–	11.6	7.0	2.5	6.8
C <sub>3</sub> A/C <sub>4</sub> AF	–	–	2.7	1.1	0.4	1.9
Amorphous <sup>1</sup>	28.4*	45.0*	–	–	88.7**	25.2***

<sup>1</sup> Amorphous can be \*pozzolanic material associated to a pronounced scattering hump; \*\* pozzolanic material associated to a pronounced scattering hump and clay minerals; \*\*\*clay with smectitic composition.

of montmorillonite, whose collapsing low-angle peak may be induced by a heating cycle to reduce the moisture content. Montmorillonite is a 2:1 clay with dioctahedral structure belonging to the smectite group. The ability in holding water within the interlayer, as a result of the weak bond of interlayer cations to the T-O-T sheets, makes montmorillonite expansive. Simulations have reported that just 4% moisture content within montmorillonite is sufficient to allow the interlayer to swell during hydration [70].

Cement phases were present in RF, FSB, LS and in a lesser extent in

HBG. Those phases comprised small amounts of gypsum and moderate amounts of cement clinker formed by calcium-silicates (C<sub>3</sub>S and C<sub>2</sub>S) and calcium-aluminates (C<sub>3</sub>A and C<sub>4</sub>AF) phases [71]. The reactive clinker fraction was close to 15 wt% in RF, slightly lower than 10 wt% in FSB and LS, and around 3 wt% in HBG.

The amorphous phase mentioned in Table 1 stands for the pozzolanic components present in BF, MP and HBG. HBG was formed by pozzolanic and clay phase either, while LS can be considered mostly clayey. The clay minerals in HBG and LS, which showed a low crystallinity, were described with peak-phases and still considered as amorphous.

### 3.2. Calorimetric behaviour

Time-dependent calorimetric curves pertaining to the cumulative heat release over grouts hydration are shown in Fig. 4. The heat at any time over the first 36 h of hydration, expressed in J·g<sup>-1</sup>, was assumed proportional to the degree of reaction of the grouts. The BF, RF, FSB and HBG grouts exhibited similar shape of the curves and final heat emitted above 4 J·g<sup>-1</sup> and up to 13 J·g<sup>-1</sup>. Whereas the MP and LS grouts were characterized by a slower and faster heat development than the former grouts, respectively. The common aspect of all grouts was the relatively low reactivity if compared with a CEM-I Portland cement hydration, which involves exothermic reactions that, among 24 and 72 h, may produce heat around 250 J·g<sup>-1</sup>, as function of the water-to-solid ratio (w/s) [72].

The calorimetric behaviour of the grouts may be ascribed to their phase composition (Table 1), with prevailing inert or pozzolanic

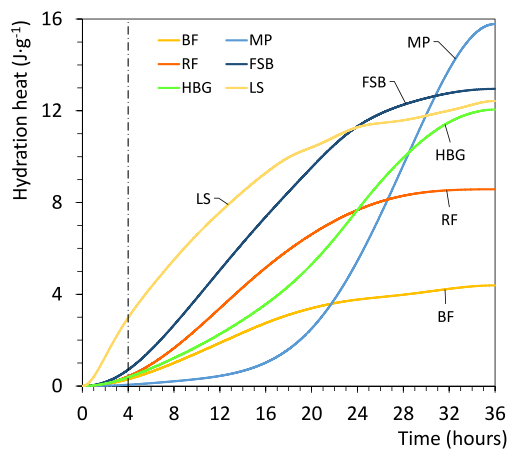


Fig. 4. Calorimetric hydration curves of all grouts at recommended w/s ratio.

**Table 2**

Main calorimetric outcomes concerning the hydration of the grouts: final adiabatic temperature, full power output, and time required to reach this power.

Calorimetric outcomes	BF	MP	RF	FSB	HBG	LS
Temperature at 36 h (°C)	26.5	33.5	27.8	30.4	29.0	29.0
Full power output (mW·g <sup>-1</sup> )	0.06	0.30	0.13	0.16	0.17	0.25
Time to reach the power (hours)	12	28	12	10	23	2

constituents, as well as the w/s ratio used and recommended by the relevant datasheets. The final adiabatic temperature after 36 h, which corresponded to the differential temperature increment starting from an initial value of about 23.4 °C after mixing, the full power output and the time required to reach it, are reported in Table 2. All grouts presented an adiabatic temperature plateau smaller than 50 °C (Fig. 4), which is in line with the selection criteria adopted in [73]. Furthermore, all grouts reached the full power output within the 36 h of monitoring. The time required to reach this power might provide an estimation of the length of the setting. Vicat needle [74] and penetration [75] tests are commonly used to assess the setting time of cement paste and concrete respectively. The initial and final setting time of cement and mortar were recently estimated by calorimetry data fitting [76]. Differences between each test protocol may occur. In this work, we focused in selecting a criterion based on heat of hydration (Fig. 4) and calorimetric outcomes (Table 2).

The experimental outcomes indicated that all grouts, except for LS, could allow adequate working times of at least 4 h that was one of the initial pre-requisites. In LS, filler and water absorption effects of montmorillonite may account for the accelerated hydration of this paste.

Moreover, a longer curing period than the common 28 days was preferred before compression tests owing to the slow reactivity of the grouts [48,57,58].

**Table 3**

Average apparent densities and volumetric shrinkage plus or minus one standard deviation.

Grout	w/s ratio	Density of fresh grout (kg/l)*	Density of hardened moist grout (kg/l)	Density of hardened dry grout (kg/l)	Volumetric shrinkage (%)
BF	0.35	1.87	1.962 ± 0.013	1.654 ± 0.082	3.96 ± 1.96
MP	0.35	1.85	1.937 ± 0.022	1.564 ± 0.085	1.33 ± 1.15
RF	0.48	1.68	1.683 ± 0.030	1.213 ± 0.009	3.64 ± 1.14
FSB	0.45	1.72	1.796 ± 0.010	1.292 ± 0.013	1.99 ± 0.99
HBG-0.8	0.80	1.46	1.595 ± 0.001	1.082 ± 0.015	11.23 ± 2.06
HBG-0.7	0.70	1.48	1.610 ± 0.002	1.112 ± 0.013	5.94 ± 2.74
HBG-0.6	0.60	1.50	1.661 ± 0.041	1.164 ± 0.012	3.50 ± 0.71
LS-0.9	0.90	1.56	1.570 ± 0.007	0.932 ± 0.013	14.62 ± 0.84
LS-0.8	0.80	1.58	1.577 ± 0.044	0.964 ± 0.014	10.67 ± 1.15
LS-0.7	0.70	1.63	1.616 ± 0.044	1.050 ± 0.013	6.29 ± 1.46
LS-0.6	0.60	1.72	1.738 ± 0.013	1.245 ± 0.015	4.64 ± 0.55

\* measurement error of about ±1%.

### 3.3. Density characterization

The average apparent densities of the grouts in their fresh and hardened states are reported in Table 3 with the corresponding mixing w/s ratio. The preferred w/s ratio was that recommended by the relevant datasheet and reported as the first value in Table 3. The measured densities of fresh grouts varied slightly from the hardened moist densities of the grouts. More significant was the difference between the moist and dry densities of the hardened samples.

Measuring the density of the fresh grout was instrumental for the onsite installation of a geothermal probe designed within the GEO4-CIVIC project [16]. In the pilot test site in Padova (Italy), a stainless-steel coaxial probe was installed with the new drilling method defined in the project up to about 90 m depth [13]. In practice, the density of fresh grout shall be less than the gross apparent density of the probe to avoid any possible buoyancy of the same. In our case, the gross apparent density of the probe was of 0.83 kg/l, in case the stainless-steel pipe was empty, or 1.75 kg/l when the pipe was ballasted with water during installation.

All the grouts, apart BF and MP, met this onsite installation requirement. Moreover, the installation required pumpable geothermal grouts, which typically are characterised by a density of 1450–1900 kg/m<sup>3</sup> [33,49,73], as those tested (Table 3). The density of the hardened dry grouts was also useful for an assessment of the amount of water possibly trapped in the hardened mixtures in moist conditions as those that can be found onsite under the water table and that can influence the thermal conductivity [34].

Lastly, an appraisal of a nominal volumetric shrinkage of the hardened grouts is also given in Table 3. Three cubic formworks full to the brim were prepared per each mixture. The shrinkage was calculated on moist cured samples as the percentage reduction of the volume from that of the 50 mm nominal cubic formworks [48]. The volumetric shrinkage provided a first appraisal of the material stability, which was successively more thoroughly examined via the bleeding test [52]. HBG and LS grouts showed shrinkages of more than 11% when mixed with the recommended w/s ratio. Therefore, few additional reduced w/s ratios were considered until reaching a still workable mix and a visually stable volume (Table 3). As possible comparison, the ACI 229R-13 [49] reports linear shrinkage values of 1 or 2% for acceptable fluid CLSM mixtures with high water contents. These linear values correspond to a volumetric shrinkage of 3 or 6%, respectively. The HGB grout with a w/s of 0.8 as well as the LS grout with w/s of 0.9 and 0.8 were those not complying with the former parameters and showing an excessive volume shrinkage. HGB and LS grouts with w/s of 0.7 showed a residual volume shrinkage, while both had a visually stable volume at w/s of 0.6. Nonetheless, the volumetric stability was attained at the cost of a reduced workability and flowability of the grouts. On the other hand, BF, MP, RF, and FSB offered a stable volumetric appearance when mixed with the recommended w/s ratio as confirmed by the data reported in Table 3.

### 3.4. Bleeding performance

The BF, MP, RF and FSB grouts presented an acceptable volumetric stability in their hardened state without showing any significant bleeding. On the other hand, LS and HBG were affected by a noticeable bleeding potential as anticipated in section 3.3. Consequently, the bleeding volume percentage of LS and HBG at different w/s ratios was further examined according to ASTM C940–16 [52]. The bleeding curves during the first 120 min after mixing are shown in Fig. 5.

The bleeding percentages at 120 min for LS-0.9 and HBG-0.8 were of 11% and 10.7%, respectively. The bleeding decreased when the water was reduced in the mixes. LS grout with w/s of 0.8, 0.7 and 0.6 showed a bleeding of 8%, 2.5% and 2%, respectively. HBG grout with a w/s of 0.7 had a bleeding of 6%. HBG grout with a w/s of 0.6 was poorly workable and did not show a measurable bleeding. Interestingly, grouts with a volumetric shrinkage lower than 4% (Table 3) delivered a visually stable volume, which was confirmed by the bleeding tests. A volumetric shrinkage upper bound of 4% might be an appropriate threshold for stable grouts.

Geothermal grouts are usually considered volumetrically stable when the bleeding percentage is smaller than a certain target. A maximum 5% bleeding in 2 h was indicated in [53]. This target value was often considered in other studies [51,54,77]. Nonetheless, a more demanding target as lower as 2% might be more appropriate for delivering overall better physico-mechanical properties [20,51,78]. In fact, a surplus of free water is usually connected with an increment of material porosity and water permeability, and a reduction of thermal conductivity and durability [20,36,79,80]. Future studies will investigate these aspects.

Noteworthy, the 2% target is also typical for structural grouts that are subjected to stringent physico-mechanical requirements [81,82]. This last bleeding percentage target might be appropriate for geothermal grouts as well and was preferred also in [73,83].

### 3.5. Thermal conductivity

The thermal conductivity of the grout plays a key role in determining the borehole thermal resistance (BTR), namely the thermal resistance between the fluid in the probe and the borehole wall, and in impacting the BHEs efficiency [84,85]. Borehole backfilling grouts regulate the heat transfer between the heat exchanger and the surrounding ground. The higher the thermal conductivity of the grout, the lower the BTR [86]. In addition, using thermally enhanced backfilling material, a better performance of the GSHP systems is expected, as well as a shortening of the required bore length associated with a reduction of installation costs [31].

Borehole thermal resistance is more important for GSHP performance during short, transient, heat pulses, while rock-sediment thermal conductivity becomes more important for longer-term, sustained operation [87,88]. Therefore, the grout thermal properties affect the heat transfer process especially in the transient regime, for example considering an hourly response to the building variable thermal loads, where subsequent cycles of switching the system on and off are planned. In this framework, the grout thermal resistance greatly affects the overall borehole heat exchange and, the use of a thermally enhanced mixture can optimize the system response to variable thermal loads [89]. Consequently, grouts with higher thermal conductivity are sought after because they can significantly reduce the BTR in the early stage of GSHPs operation. However, an excessive increase in thermal conductivity could not lead to a substantial decrease of the BTR, as desired, because it is the result of an interplay between several factors as probe geometry, borehole diameter, grout thickness and grout thermal conductivity. Therefore, the selection of a suitable backfill material should not only consider an improvement of the heat transfer with consequent reduction of the BTR, but also the whole grout properties described in this paper, the operating conditions, the technological solutions selected for GSHPs, the geological and hydrogeological characteristic, the thermal needs of the systems, and the economic conditions [22,30,31]. Moreover, an excellent grout for geothermal application must ensure not only a balanced thermal exchange with the subsoil, but also guarantee the resistance and flexibility to underground stress and hydraulic sealing capacities.

The data about the average thermal conductivity ( $\lambda$ ) of dry and water saturated specimens (as specified in section 2.7) is reported in Table 4 and Fig. 6 for the grouts mixed with datasheet recommended w/s ratios. In dry conditions the mean  $\lambda$  value for each mixture was smaller than  $0.60 \text{ Wm}^{-1}\text{K}^{-1}$ , typical of a dry soil material [90]. The minimum ( $0.20 \text{ Wm}^{-1}\text{K}^{-1}$ ) and maximum ( $0.57 \text{ Wm}^{-1}\text{K}^{-1}$ ) values belong to LS and BF, respectively. The possible gain in thermal conductivity for LS and HBG

**Table 4**

Dry and water saturated thermal conductivity plus or minus one standard deviation and porosity values.

Material	Dry thermal conductivity ( $\text{Wm}^{-1}\text{K}^{-1}$ )	Wet thermal conductivity ( $\text{Wm}^{-1}\text{K}^{-1}$ )	Total porosity ( $\Phi$ ) (%)
BF	$0.57 \pm 0.016$	$1.63 \pm 0.033$	30
MP	$0.49 \pm 0.008$	$1.44 \pm 0.018$	33
RF	$0.27 \pm 0.009$	$1.39 \pm 0.026$	53
FSB	$0.36 \pm 0.005$	$1.58 \pm 0.066$	48
HBG-0.8	$0.27 \pm 0.045$	$2.55 \pm 0.406$	56
LS-0.9	$0.20 \pm 0.007$	$1.47 \pm 0.017$	65

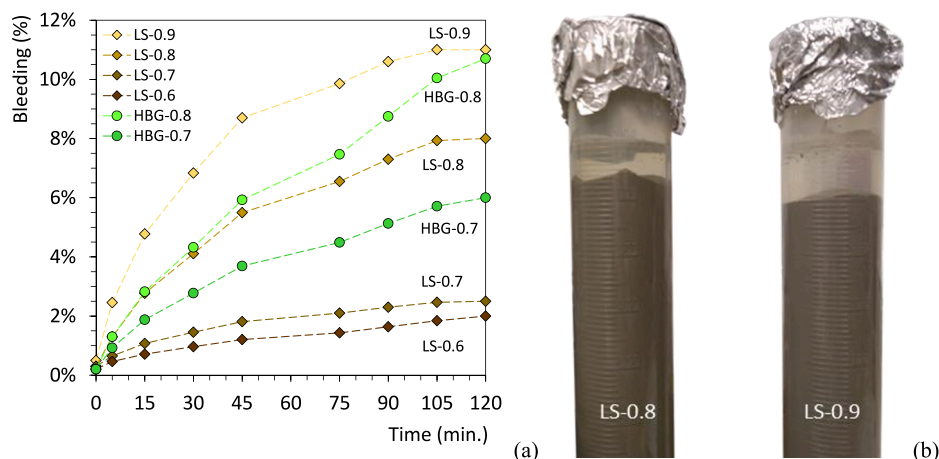


**Fig. 5.** Bleeding percentage curves for the LS and HBG grouts at different w/s ratios (a), and two samples of LS grout during bleeding test (b).

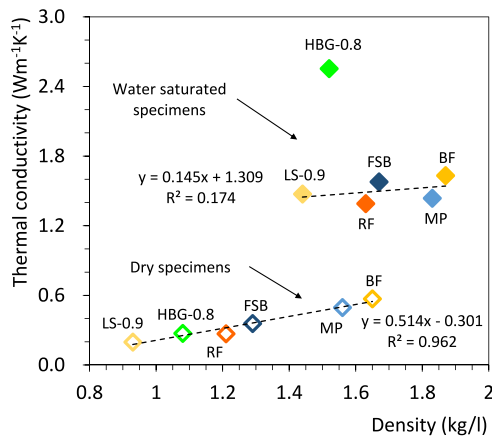


Fig. 6. Dry and water saturated thermal conductivities of the grouts and related trendlines.

grouts at reduced w/s ratios might be estimated using the trendlines of Fig. 6 and the relevant densities of Table 3. The possible gain for dry LS and HBG grouts at w/s of 0.6 was about 11% and 7%, respectively.

For water saturated conditions  $\lambda$  values ranged between 1.39 (RF) and 2.55 (HBG)  $\text{Wm}^{-1}\text{K}^{-1}$ , with most products having a value of about 1.50  $\text{Wm}^{-1}\text{K}^{-1}$ . The increase in  $\lambda$  from dry to water saturated conditions was consistent with the total porosity values determined using the Archimedes' principle (Table 4). The grouts showed porosities ranging from 30 to 65%. The void presence was directly related to the noteworthy increase of the heat transfer capacity when the specimens undergo water saturation. In fact, when the air in the pore system is gradually replaced by a small amount of water, the contact conditions within the samples are improved dramatically leading to a sudden increase of the thermal conduction [23,90,91,92,93]. The RF, FSB, HBG-0.8, LS-0.9 saturated samples, with a total porosity close to or larger than 50% and dry  $\lambda$  values comparable to those of air ( $0.20 \text{ Wm}^{-1}\text{K}^{-1}$ ), showed the highest gain in thermal exchange capacity after water saturation, followed by the BF and MP saturated samples, characterized by 30% total porosity and dry  $\lambda$  values similar to water ( $0.56 \text{ Wm}^{-1}\text{K}^{-1}$ ). However, the presence of additives in the mixture, as graphite, contributed also to the general improvement of the thermal performance [23,90].

The possible gain for the LS-0.6 grout at w/s of 0.6 was estimated at about 4%. Whereas, for the HBG-0.6 it can be reasonable to assume a

similar thermal conductivity of HBG-0.8 owing to the marked presence of graphite. Noteworthy, wet measurements reflect the thermal properties of grouts in onsite wet environments more closely. The wet thermal conductivities were from about 3 (BF and MF) to 9 (HBG) times larger than the related dry values. Among these, the proneness of HBG to heat transfer ( $2.55 \text{ Wm}^{-1}\text{K}^{-1}$ ) was reasonably related to the presence of highly heat conductive graphite (Table 1).

### 3.6. Compressive strength

The compressive strengths of the grouts, including those with reduced w/s ratio, are presented in Fig. 7 with related error bars (plus or minus one standard deviation). The grouts were tested in moist conditions after 56 days of curing. The average cubic compressive strengths spanned between 0.41 MPa of the LS-0.9 and 23.22 MPa of the MP grout. The reduction of the w/s ratio resulted in improved mechanical performances for LS and HBG grouts.

Grouts aimed at shallow geothermal applications do not need high mechanical performances. Accordingly, the compressive strength, which is often considered a secondary physico-mechanical parameter, is checked after studying other thermo-physic aspects such as thermal conductivity, durability to cyclic thermal loads and water permeability [8,20,21,30]. Nonetheless, a minimum compressive strength is evidently necessary for the borehole stability. As lower bound, a minimum compressive strength of 1 MPa was preliminary indicated in [73]. Moreover, shallow geothermal grouts probably do not need to attain the compressive strength of 6.9 MPa that is usually required as minimum strength for deeper geothermal wells [35,94,95]. Additionally, the use of low strength grouts, which usually possess a lower modulus of elasticity and an enhanced deformability [79,80], can favour the accommodation of volume variations during operation of the geothermal probes due to thermal cyclic loads, and the consequent reduction of stress concentrations and cracking proneness of the backfill material as highlighted by the structural analysis of geothermal wells in [35]. The reduction of backfill material cracking is favourable for a better water permeability performance and durability of the installation. Lastly, the use of low strength backfills can permit a possible future rework of the installation. In fact, flowable CLSM mixtures [49], also used as geotechnical backfills [50,51], should have a compressive strength lower than 8.3 MPa. In particular, the future excavatability is possible with mechanical equipment when the compressive strength does not exceed 2.1 MPa [49]. Consequently, the compressive strength range of 1 to 6.9 MPa appears advisable for shallow geothermal grouts, with possible preference for the range of 1 to 2.1 MPa.

Accordingly, the BF and MP grouts reached an excessive compressive

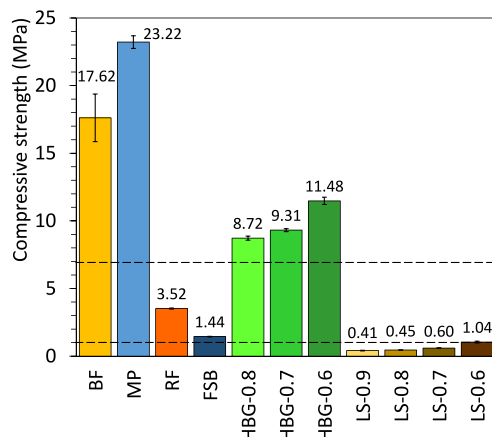


Fig. 7. Average cubic compressive strengths of the grouts plus or minus one standard deviation (a), RF grout samples before compression tests (b), and FSB samples after testing presenting the typical hourglass failure surface (c).

strength, besides being the heaviest and not meeting the practical installation requirement of section 3.3, and not having a clear advantage in the wet thermal conductivity over the lower strength grouts. All the HBG grouts had a compressive performance larger than the advisable strength range. The LS grout barely reached the minimum compressive strength of 1 MPa only when the w/s was reduced to 0.6. Therefore, according to the previous experimental outcomes, the BF, MP, HBG and LS grouts still need further studies for a finer optimization of their composition to suit the preferred physico-mechanical performances. This optimization was beyond the scopes of the present work and will be the subject of future investigations. The RF and FSB grouts closely matched, without further refinements, the favourite compressive strength range, besides having showed suitable results also for all the previous thermo-physical properties.

### 3.7. Flowability and rheology properties

The RF and FSB grouts showed the best combination of physico-mechanical performances. Therefore, the investigation focused on the determination of their flowability and rheological properties, which were useful for describing their pumpability.

The flow curves, obtained with the EN 445 [59] cone during the first 4 h of ambient temperature curing, are shown in Fig. 8a. The flow times and the rheological parameters are given in Table 5. The 4-hour monitoring window corresponded to the desired onsite probe installation time set in the GEO4CIVHIC project [16]. The RF curve presented an exponential trend with a thickening of the grout after 2 h, time beyond which the viscosity rapidly increased with a reduction of flowability. The FSB curve had a softer exponential trend and qualitatively appeared flowable during the entire 4-hour window.

Customarily, commercial optimised grouts for low-enthalpy geothermal systems have an EN 445 [59] flow time range of 45 to 100 s [33]. Nonetheless, an explicit flowability acceptance criterion for shallow geothermal grouts was not yet available and a preliminary maximum flow time range of 45 to 60 s was indicated in [59]. A clear flowability acceptance criterion existed for CLSM mixtures [49] that were also successfully used for shallow geothermal systems in [50,51,78]. Flowable CLSM mixtures should have a flow time smaller than  $30 \pm 5$  s [49]. Nonetheless, the flow times in [49] are determined according to the ASTM C939/C939M-16a [62], which makes use of a different and larger cone than the EN 445 [59]. Therefore, an empirical conversion correlation for the efflux of 1 L of grout from the two different cones was derived in Fig. 8b by using the data of [96,97]. The criterion for CLSM [49] would correspond to a flow time smaller than  $60 \pm 15$  s from an EN 445 [59] cone. Consequently, the converted

maximum flow time range was highlighted in Fig. 8a, together with a possible upper bound set at 100 s, which corresponded to the practical annotation of [33]. According to these bounds, the FSB grout was acceptably flowable during the entire 4-hour window, whereas the RF was acceptably flowable for about 1 h and 40 min and attained the upper bound at about 2 h and 15 min.

The shear curves of the RF and FSB grouts were recorded at every hour of the former 4-hour window as done for the flowability tests (Fig. 9). The grouts exhibited the typical time-dependent Non-Newtonian flow of cementitious and geotechnical fluid mixtures [38,64,98,99]. The rheological behaviour of RF and FSB grouts was fitted with the Herschel-Bulkley and the Bingham models (Table 5). The FSB grout, during the first hour after mixing, practically showed a linear behaviour that could be accurately described by the Bingham model. Whereas the rheological behaviour of the following hours could be described by both models. The RF grout always showed a non-linear behaviour and the rheological data was fitted with both models during the 4-hour window.

The RF grout presented larger apparent plastic viscosity values, over the 4-hour window, than the FSB grout, as was expected from the flow cone data. Moreover, the RF grout had also larger yield stress values than the FSB grout. This pointed out that the RF grout had a possible better washout resistance, according to [100], than the FSB. Consequently, the RF grout was more suitable for shorter shallow geothermal systems installations in presence of groundwater, while the FSB grout was better suited for prolonged and drier onsite installations.

Pumpable geotechnical grouts for rock grouting should have a maximum yield stress within 32 and 43 Pa, and an apparent plastic viscosity lower than 0.1 Pa-s [99]. Cement pastes for structural grouts can have yield stress values ranging from 1 to 26 Pa and apparent viscosity ranging from 0.10 to 0.32 Pa-s, while the related pumpable self-compacting mortars can have a yield stress ranging from 7 to 88 Pa, and an apparent viscosity ranging from 3.7 to 10.7 Pa-s [101]. These practical ranges might be considered as the lower and upper pumpability bounds for geothermal grouts, respectively. The Bingham model data of Table 5 are mostly within the former ranges apart for the RF grout after 3 h from mixing.

Possible more refined maximum acceptance ranges for geothermal grouts can be proposed based on Fig. 10, where the Bingham yield stress and the apparent viscosity values of Table 5 were plotted versus the EN 445 [59] flow times. Data concerning flowable and pumpable grouts retrieved from literature [60,98–105] was added in Fig. 10 to strengthen the correlation curves. The lower and upper bounds of the preferred maximum flow time range (Fig. 8) would correspond to apparent viscosities of 0.47 and 0.58 Pa-s, respectively (Fig. 10a). The flow time

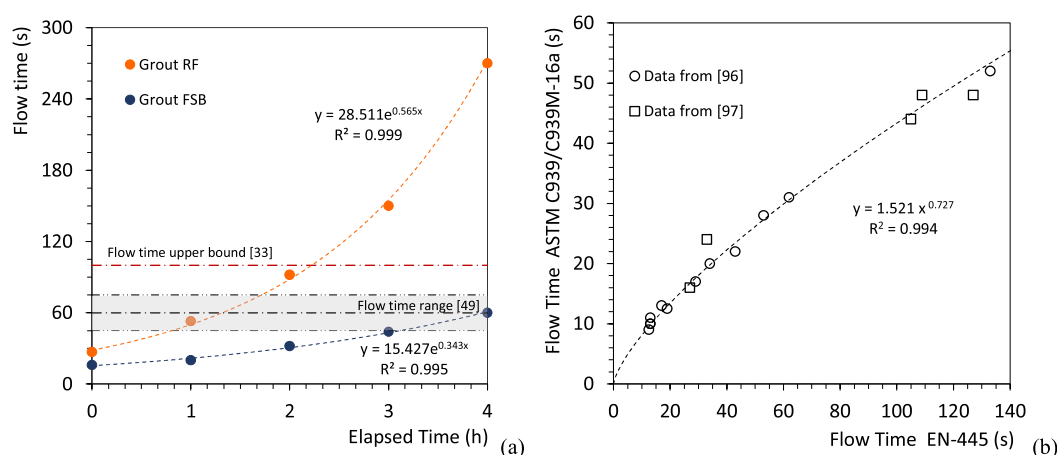
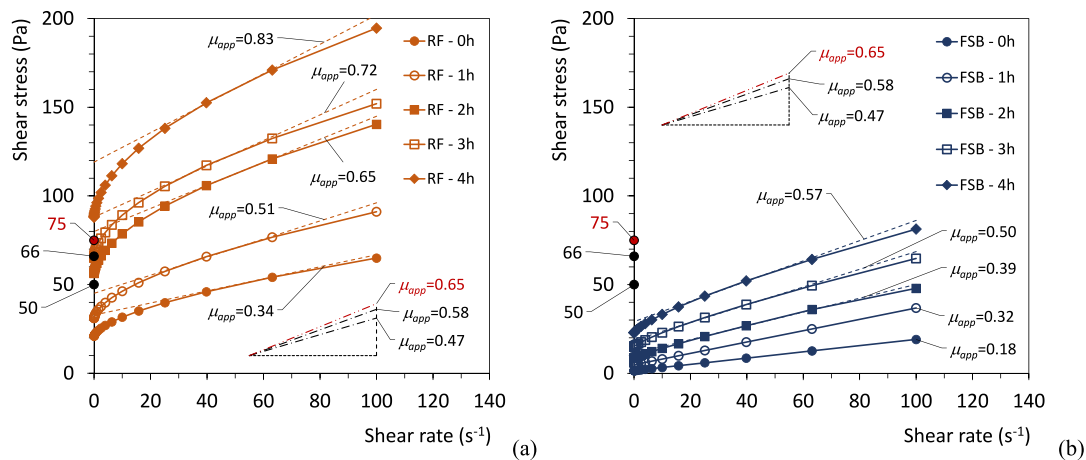


Fig. 8. (a) EN 445 [59] flowability test for RF and FSB grouts, and (b) correlation between the flow times of the EN 445 [59] and ASTM C939/C939M-16a [62] cone apparatuses.

**Table 5**  
Rheological properties of RF and FSB grouts.

Grout	Time (hours)	Flow time (s)	Herschel-Bulkley model			Bingham model	
			Cohesion (Pa)	Consistency index (Pa·s)	Flow index	Yield stress (Pa)	Apparent Plastic viscosity (Pa·s)
RF	0	27	20.80	2.66	0.61	32.83	0.34
	1	53	30.80	3.98	0.59	45.08	0.51
	2	92	55.88	6.12	0.57	79.93	0.65
	3	150	64.52	6.95	0.55	88.06	0.72
	4	270	87.23	8.83	0.54	119.07	0.83
FSB	0	16	–	–	–	1.50	0.18
	1	20	–	–	–	4.80	0.32
	2	32	8.76	0.68	0.88	11.12	0.39
	3	44	14.96	1.25	0.80	18.62	0.50
	4	60	22.79	1.85	0.75	29.14	0.57



**Fig. 9.** Shear stress versus shear rate curves for RF (a) and FSB (b) grouts during the first 4 h. Thresholds for the yield stress are pinpointed on the y-axis, while thresholds for the apparent viscosity are presented as dotted slopes.

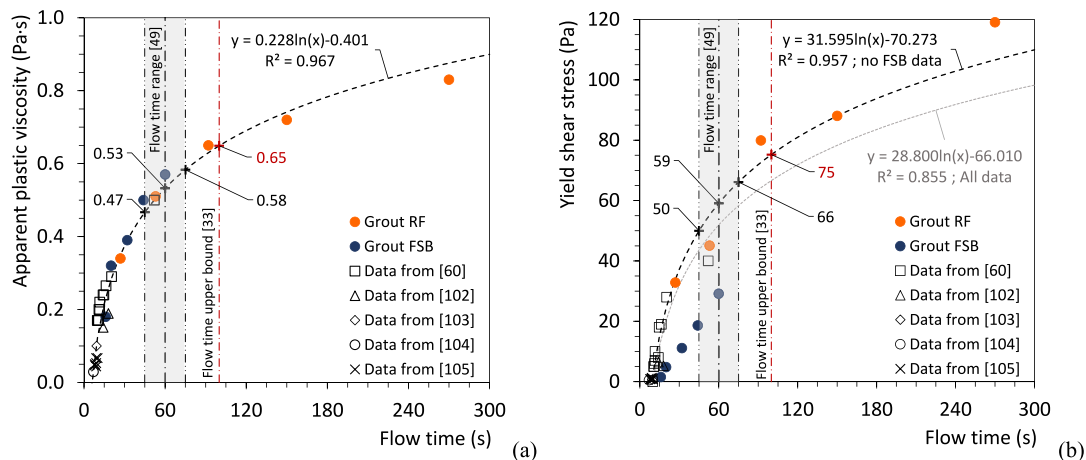


**Fig. 10.** Bingham apparent plastic viscosity (a) and yield shear stress (b) versus flow time.

upper bound of 100 s would suggest a maximum apparent viscosity of 0.65 Pa·s.

Yield stress values should be small enough to assure that the flow will be initiated [60]. After this occurrence, the apparent viscosity will control the flow behaviour of the grout [60]. Our experimental and literature data [60,102–105] showed that fluid shear-thinning grouts (e.g. RF) tend to have larger yield stresses than grouts that are practically Bingham fluids (e.g. FSB). Therefore, the thresholds can be set over shear-thinning grout data thus, the lower and upper bounds of the preferred maximum flow time range would correspond to yield stresses

of 50 and 66 Pa, respectively (Fig. 10b). The flow time upper bound of 100 s would suggest a maximum yield stress of 75 Pa.

According to the geothermal acceptance ranges, the FSB grout was pumpable for the entire 4-hour window of our preferred working time, whereas the RF grout practically reached the pumpability acceptance criteria after 2 h of elapsed time from mixing (Fig. 9 and Table 5).

**4. Brief cost analysis**

A brief survey was conducted at local retail shops for construction

materials in Italy between 2019 and 2020. The cost ranges largely depend on the possibility of purchasing the materials in small (i.e. a few hundred kilograms of product in bags of 20/25 kg) or large (i.e. big bags of 1 tonne) quantities. Temporary discounts were disregarded from the analysis of the retail costs.

Until December 2020, four out of six geothermal grouts meet, at least in part, the preferred cost target of 0.45 €/kg (see section 2.1). The retail cost ranges of the grouts were: of about 0.85–0.95 €/kg for both BF and MP, 0.36–0.39 €/kg for RF, 0.43–0.48 €/kg for FSB, 0.41–0.49 €/kg for HBG, and 0.38–0.43 €/kg for LS.

The cost of BF and MP was almost double of the preferred target. Nonetheless, these two grouts had also the largest compressive strengths and they can be further optimised with the addition of fine aggregates and admixtures to possibly halving their cost and reducing their strength within the preferred range while attaining the desired flowability. Preliminary modification trials of BF and MP grouts pointed out the feasibility of reaching a retail cost as low as 0.35 €/kg.

## 5. Conclusions

The mineralogical composition, heat of hydration, density, shrinkage, thermal conductivity, compressive strength and flowability of six commercial grouts available on the Italian construction market were investigated. Two of the six tested grouts showed the best combination of different material properties necessary for a successful thermal coupling of a BHE with the underground. The other four products showed interesting optimisation potential that will be useful for future research.

The acceptance criteria concerning grouts for shallow geothermal heat exchangers defined in this research were: a working time of at least 4 h, a water bleeding target of 2% and a volumetric shrinkage upper bound of 4%, a thermal conductivity in water saturated conditions of at least 1.4 to 1.5 Wm<sup>-1</sup>K<sup>-1</sup>, a preferred compressive strength range of 1 to 2.1 MPa, a flow time range of 60 ± 15 s.

In detail, for the preliminary selection of backfill grout for shallow geothermal systems the research highlighted that:

- The mineralogical composition was a key parameter. The use of cement grouts (RF, FSB) appeared promising in our case due to the positive outcomes of all the tests performed. These materials showed a cement clinker fraction close to or lower than 15 wt% and are mostly made of calcium carbonate, which may improve the fresh-state stability. On the other hand, the introduction of water absorbing clays above 20 wt% on cement grouts, as with LS, may present accelerated heat of hydration, water bleeding above 10%, volumetric shrinkages above 11% and mechanical strength below 1 MPa with the recommended w/s.
- The calorimetric behaviour is fundamental for ensuring an adequate working time in situ. In fact, the time of full heat output provides an estimation of the length of the setting. A working time of at least 4 h was identified as necessary for a smooth onsite installation of shallow geothermal probes. All the grouts, except for LS, respected this condition. LS exhibited the full heat output at 2 h, while the other grouts achieved their upper limit no earlier than 10 h. MP and HBG were appealing for their slower heat development, while BF for the lower full heat output.
- The density of the fresh grout was considered to avoid any possible buoyancy effect of the geothermal probe when inserted within the grout. A value of 1.75 kg/l, corresponding to the GEO4CIVHIC coaxial stainless probe ballasted with water, was set as our upper limit for the selection of a suitable grout. In this regard, the fresh RF, FSB, HBG and LS grouts complied with the density requirement, whereas BF and MP grouts showed values greater than the upper limit.
- Volumetrically stable geothermal grouts ensure better physical–mechanical properties over time. Therefore, a maximum bleeding target of 2% was recommended as an acceptance criterion

for geothermal grouts. The HBG and LS products had a marked bleeding at fresh state (greater than 2%) leading to an excessive volumetric shrinkage at hardened state (greater than 4%). The simple reduction of the w/s ratio was not sufficient for optimising the volumetric stability of these grouts. Conversely, BF, MP, RF and FSB grouts were volumetrically stable.

- Better performance of GSHP systems is expected when the grouts provide a good heat transfer between the BHE and the surrounding soil, that is the thermal conductivity in water saturated conditions is at least 1.4 to 1.5 Wm<sup>-1</sup>K<sup>-1</sup>. According to the laboratory measurements, the recorded values in water saturated conditions for the whole set of samples were in the range 1.39 to 2.55 Wm<sup>-1</sup>K<sup>-1</sup>. In detail, RF and FSB grouts presented thermal conductivities in agreement with the requirements for an efficient functioning of the coaxial geothermal probes. The HBG grout stood out given the presence of graphite.
- A preferred compressive strength range of 1 to 2.1 MPa was identified for shallow geothermal grouts out of a wider selected advisable range (1 to 6.9 MPa) derived from scientific literature. This mechanical property ensures borehole stability and is related to grout flowability and pumpability, parameters that play a key role in field applications. In detail, BF, MP and HBG grouts had compressive strengths that largely exceeded the advisable range. The LS grout hardly reached the lower bound of 1 MPa only when the w/s was reduced to 0.6. RF and FSB grouts closely matched the preferred compressive strength range. Therefore, they were selected for in situ applications.
- Summarizing, since RF and FSB grouts showed the best combination of thermo–physical–mechanical performances, the investigation focused on the determination of their flowability and rheological properties, which were useful for describing their pumpability within our preferred working time of 4 h. The preferred maximum flow time range was set to 60 ± 15 s. This flow time range was fully exploited after 1 h and 40 min and after 4 h by RF and FSB grouts, respectively. In addition, the identified acceptance ranges for the Bingham model suggested a preferred use of RF and FSB grouts within 2 and 4 h of elapsed time from mixing, respectively.
- The maximum retail cost target of 0.45 €/kg established within the EU GEO4CIVHIC project was also met by FSB and RF.

On the basis of the current experimental outcomes, the FSB appeared to be a fluid grout with the best combination of competitive thermo-physical properties and the RF grout was the second best.

The main advantages of this study consist in providing a practical overview on how to identify optimal grouts for BHE installations, able to promote an efficient thermal coupling between the borehole wall lithology and the heat exchanger, the borehole stability and the zonal sealing of the wellbore. Low enthalpy geothermal systems, which can be installed anywhere with adequate knowledge of the underground, will play a key role in the energy market in the near future due to the increasing interest towards cost-effective renewable and clean energy sources for building air-conditioning. Therefore, the selection of a proper grout will be a fundamental step in ensuring the long-term performance of these systems.

The proposed approach might have a bottleneck in the curing period necessary for grout hardening. We preferred an extended curing period of 56 days due to the possible low strength and pozzolanic composition of some grouts tested. Nonetheless, our outcomes highlighted that the use of cement grouts appeared promising, thus the typical 28 days curing period can be considered for future research. Moreover, the test plan can be designed so that several characterization tests can be run in parallel while awaiting the hardened grout samples.

Lastly, the experience gathered in preliminary installations of 100-metre long BHE suggested that the scalability and preservation of the thermo-physical properties from laboratory to onsite conditions will require further studies since they are affected by operational difficulties

related to the larger scale onsite facilities and the installation procedures (e.g. grout mixers, grout pumping and casting procedures), weather variability and geological complexity of the underground (e.g. ground-water flow, methane occurrence).

## Funding

GEO4CIVHIC project has received funding from the European Union's Horizon 2020 Research and Innovation Program under grant agreement No. 792355.

## CRedit authorship contribution statement

**Ludovico Mascarin:** Investigation, Formal analysis, Conceptualization, Writing – original draft, Writing – review & editing. **Enrico Garbin:** Conceptualization, Methodology, Investigation, Formal analysis, Validation, Writing – review & editing, Visualization. **Eloisa Di Sipio:** Data curation, Visualization, Writing – review & editing. **Giorgia Dalla Santa:** Validation. **David Bertermann:** Investigation. **Gilberto Artioli:** Resources, Supervision. **Adriana Bernardi:** Funding acquisition, Project administration. **Antonio Galgaro:** Supervision, Funding acquisition, Project administration.

## Declaration of Competing Interest

The authors declare that they have no known competing financial interests or personal relationships that could have appeared to influence the work reported in this paper.

## Acknowledgements

The authors are grateful to the Italian and international manufacturers of chemicals and construction products for the building industry that supported the present research by supplying some of the materials free of charge.

## References

- [1] M.L. Allan, S.P. Kavanaugh, Thermal conductivity of cementitious grouts and impact on heat exchanger length design for ground source heat pumps, HVAC&R Res. 5 (2) (1999) 85–96, <https://doi.org/10.1080/10789669.1999.10391226>.
- [2] S. Erol, B. François, Efficiency of various grouting materials for borehole heat exchangers, Appl. Therm. Eng. 70 (1) (2014) 788–799, <https://doi.org/10.1016/j.applthermaleng.2014.05.034>.
- [3] J. Ahn, J. Jung, Effects of fine particles on thermal conductivity of mixed silica sands, Appl. Sci. 7 (7) (2017) 650, <https://doi.org/10.3390/app7070650>.
- [4] J. Luo, Z. Luo, J. Xie, D. Xia, W. Huang, H. Shao, W. Xiang, J. Rohn, Investigation of shallow geothermal potentials for different types of ground source heat pump systems (GSHP) of Wuhan city in China, Renew. Energy. 118 (2018) 230–244, <https://doi.org/10.1016/j.renene.2017.11.017>.
- [5] A.M. Omer, Ground-source heat pumps systems and applications, Renew. Sust. Energy. Rev. 12 (2) (2008) 344–371, <https://doi.org/10.1016/j.rser.2006.10.003>.
- [6] G. Dalla Santa, A. Galgaro, R. Sassi, M. Cultrera, P. Scotton, J. Mueller, D. Bertermann, D. Mendrinós, R. Pasquali, R. Perego, S. Pera, E. Di Sipio, G. Cassiani, M. De Carli, A. Bernardi, An updated ground thermal properties database for GSHP applications, Geothermics 85 (2020) 101758, <https://doi.org/10.1016/j.geothermics.2019.101758>.
- [7] G. Emmi, A. Zarrella, M. De Carli, S. Moretto, A. Galgaro, M. Cultrera, M. Di Tuccio, A. Bernardi, Ground source heat pump systems in historical buildings: two Italian case studies, Energy. Proced. 133 (2017) 183–194, <https://doi.org/10.1016/j.egypro.2017.09.383>.
- [8] P. Pascual-Muñoz, I. Indacoechea-Vega, D. Zamora-Barraza, D. Castro-Fresno, Experimental analysis of enhanced cement-sand-based geothermal grouting materials, Constr. Build. Mater. 185 (2018) 481–488, <https://doi.org/10.1016/j.conbuildmat.2018.07.076>.
- [9] S.J. Self, B.V. Reddy, M.A. Rosen, Geothermal heat pump systems: Status review and comparison with other heating options, Appl. Energy. 101 (2013) 341–348, <https://doi.org/10.1016/j.apenergy.2012.01.048>.
- [10] D. Banks. *An Introduction To Thermogeology – Ground Source Heating And Cooling*, 2nd ed., Wiley-Blackwell, Chichester (West Sussex, UK), 2012.
- [11] S. Kavanaugh, K. Rafferty. *Geothermal Heating and Cooling Design of Ground-Source Heat Pump Systems*, ASHRAE, Atlanta (USA), 2014.
- [12] A. Toth, E. Bobok. *Flow and Heat Transfer in Geothermal Systems: Basic Equations for Describing and Modeling Geothermal Phenomena and Technologies*, Elsevier, Amsterdam (The Netherlands), 2017.
- [13] M.H. Ahmadi, M.A. Ahmadi, M.S. Sadaghiani, M. Ghazvini, S. Shahriar, M. Alhuyi Nazari, Ground source heat pump carbon emissions and ground-source heat pump systems for heating and cooling of buildings: a review, Environ. Prog. Sustain. 37 (4) (2018) 1241–1265, <https://doi.org/10.1002/ep.12802>.
- [14] B. Badenes, B. Sanner, M.Á. Mateo Pla, J.M. Cuevas, F. Bartoli, F. Ciardelli, R. M. González, A.N. Ghafar, P. Fontana, L. Lemus Zuñiga, J.F. Urchueguía, Development of advanced materials guided by numerical simulations to improve performance and cost-efficiency of borehole heat exchangers (BHEs), Energy 201 (2020) 117628, <https://doi.org/10.1016/j.energy.2020.117628>.
- [15] C. Karytsas, Current state of the art of geothermal heat pumps as applied to buildings, Adv. Build. Energy Res. 6 (1) (2012) 119–140, <https://doi.org/10.1080/17512549.2012.672004>.
- [16] EU GEO4CIVHIC project, Most Easy, Efficient and Low Cost Geothermal Systems for Retrofitting Civil and Historical Buildings. <https://geo4civhic.eu/>, 2021 (last access 1 March 2021).
- [17] D. Quaggiotto, A. Zarrella, G. Emmi, M. De Carli, L. Pockelé, J. Vercruysee, M. Psyk, D. Righini, A. Galgaro, D. Mendrinós, A. Bernardi, Simulation-based comparison between the thermal behavior of coaxial and double U-tube borehole heat exchangers, Energies 12 (12) (2019) 2321, <https://doi.org/10.3390/en12122321>.
- [18] J. Acuña, B. Palm, Distributed thermal response tests on pipe-in-pipe borehole heat exchangers, Appl. Energy. 109 (2013) 312–320, <https://doi.org/10.1016/j.apenergy.2013.01.024>.
- [19] J. Raymond, S. Mercier, L. Nguyen, Designing coaxial ground heat exchangers with a thermally enhanced outer pipe, Geotherm. Energy 3 (7) (2015) 14, <https://doi.org/10.1186/s40517-015-0027-3>.
- [20] I. Indacoechea-Vega, P. Pascual-Muñoz, D. Castro-Fresno, M. Calzada-Pérez, Experimental characterization and performance evaluation of geothermal grouting materials subjected to heating-cooling cycles, Constr. Build. Mater. 98 (2015) 583–592, <https://doi.org/10.1016/j.conbuildmat.2015.08.132>.
- [21] M.L. Allan, Materials characterization of superplasticized cement-sand grout, Cement. Concrete Res. 30 (6) (2000) 937–942, [https://doi.org/10.1016/S0008-8846\(00\)00275-1](https://doi.org/10.1016/S0008-8846(00)00275-1).
- [22] H. Javadi, S. Mousavi Ajarostaghi, M. Rosen, M. Pourfallah, A comprehensive review of backfill materials and their effects on ground heat exchanger performance, Sustainability 10 (2018) 1–22, <https://doi.org/10.3390/su10124486>.
- [23] E. Di Sipio, D. Bertermann, Thermal properties variations in unconsolidated material for very shallow geothermal application (ITER project), Int. Agrophys. 32 (2) (2018) 149–164, <https://doi.org/10.1515/intag-2017-0002>.
- [24] Z. Xia, R. Chen, X. Kang, Laboratory characterization and modelling of the thermal-mechanical properties of binary soil mixtures, Soils. Found. 59 (6) (2019) 2167–2179, <https://doi.org/10.1016/j.sandf.2019.11.013>.
- [25] F. Chen, J. Mao, S. Chen, C. Li, P. Hou, L. Liao, Efficiency analysis of utilizing phase change materials as grout for a vertical U-tube heat exchanger coupled ground source heat pump system, Appl. Therm. Eng. 130 (2018) 698–709, <https://doi.org/10.1016/j.applthermaleng.2017.11.062>.
- [26] Y. Lyne, H. Paksoy, M. Farid, Laboratory investigation on the use of thermally enhanced phase change material to improve the performance of borehole heat exchangers for ground source heat pumps, Int. J. Energy. Res. 43 (9) (2019) 4148–4156, <https://doi.org/10.1002/er.4522>.
- [27] M. Mahmoud, M. Ramadan, K. Pullen, M.A. Abdelkareem, T. Wilberforce, A.-G. Olabi, S. Naher, A review of grout materials in geothermal energy applications, Int. J. Thermofluids 10 (2021) 100070, <https://doi.org/10.1016/j.ijtf.2021.100070>.
- [28] J. Johansson, B. Adl-Zarrabi, Modelling and evaluation of groundwater filled boreholes subjected to natural convection, Appl. Energy. 253 (2019) 113555, <https://doi.org/10.1016/j.apenergy.2019.113555>.
- [29] A.J. Philippacopoulos, M.L. Berndt, Influence of debonding in ground heat exchangers used with geothermal heat pumps, Geothermics 30 (5) (2001) 527–545, [https://doi.org/10.1016/S0375-6505\(01\)00011-6](https://doi.org/10.1016/S0375-6505(01)00011-6).
- [30] R. Borinaga-Treviño, P. Pascual-Muñoz, D. Castro-Fresno, J.J. Del Coz-Díaz, Study of different grouting materials used in vertical geothermal closed-loop heat exchangers, Appl. Therm. Eng. 50 (1) (2013) 159–167, <https://doi.org/10.1016/j.applthermaleng.2012.05.029>.
- [31] C. Lee, K. Lee, H. Choi, H.P. Choi, Characteristics of thermally-enhanced bentonite grouts for geothermal heat exchanger in South Korea, Sci. China Ser. E 53 (1) (2010) 123–128, <https://doi.org/10.1007/s11431-009-0413-9>.
- [32] C. Sáez Blázquez, A. Farfán Martín, I. Martín Nieto, P. Carrasco García, L. S. Sánchez Pérez, D. González-Aguilera, Analysis and study of different grouting materials in vertical geothermal closed-loop systems, Renewable Energy 114 (2017) 1189–1200, <https://doi.org/10.1016/j.renene.2017.08.011>.
- [33] M. Viccaro, Doped bentonitic grouts for implementing performances of low-enthalpy geothermal systems, Geotherm. Energy 6 (4) (2018) 13, <https://doi.org/10.1186/s40517-018-0090-7>.
- [34] F. Delaleux, X. Py, R. Olives, A. Dominguez, Enhancement of geothermal borehole heat exchangers performances by improvement of bentonite grouts conductivity, Appl. Therm. Eng. 33–34 (2012) 92–99, <https://doi.org/10.1016/j.applthermaleng.2011.09.017>.
- [35] A.J. Philippacopoulos, M.L. Berndt, Structural analysis of geothermal well cements, Geothermics 31 (6) (2002) 657–676, [https://doi.org/10.1016/S0375-6505\(02\)00029-9](https://doi.org/10.1016/S0375-6505(02)00029-9).

- [36] R. Borinaga-Treviño, P. Pascual-Muñoz, M.A. Calzada-Pérez, D. Castro-Fresno, Freeze-thaw durability of cement-based geothermal grouting materials, *Constr. Build. Mater.* 55 (2014) 390–397, <https://doi.org/10.1016/j.conbuildmat.2014.01.051>.
- [37] P. Salim, M. Amani, Principal Points in Cementing Geothermal Wells, *APED* 5 (1) (2013) 77–91, <https://doi.org/10.3968/j.aped.1925543820130501.1145>.
- [38] E.B. Nelson, *Well Cementing*, Elsevier, Amsterdam (The Netherlands), 1990.
- [39] Environment Agency, Environmental Good Practice Guide for Ground Source Heating and Cooling - GEHO0311BTPA-E-E, The Environment Agency, Bristol (UK). [https://www.gshp.org.uk/pdf/EA\\_GSHC\\_Good\\_Practice\\_Guide.pdf](https://www.gshp.org.uk/pdf/EA_GSHC_Good_Practice_Guide.pdf), 2011 (accessed September 2021).
- [40] Deliverable D2.4, Simulation and design of co-axial heat exchangers with regard to performance and costs, EU GEO4CIVHIC – Most Easy, Efficient and Low Cost Geothermal Systems for Retrofitting Civil and Historical Buildings. <https://geo4civhic.eu/>, 2019 (last access 1 March 2021).
- [41] EN 12715, Execution of special geotechnical work - Grouting, European Committee for Standardization, Brussels (Belgium), 2000.
- [42] D.L. Bish, S. Howard, Quantitative phase analysis using the Rietveld method, *J. Appl. Crystallogr.* 21 (2) (1988) 86–91, <https://doi.org/10.1107/S0021889887009415>.
- [43] A.A. Coelho, TOPAS and TOPAS Academic: an optimization program integrating computer algebra and crystallographic objects written in C++, *J. Appl. Crystallogr.* 51 (1) (2018) 210–218, <https://doi.org/10.1107/S1600576718000183>.
- [44] EN 196-1, Methods of testing cement - Part 1: Determination of strength, European Committee for Standardization, Brussels (Belgium), 2005.
- [45] RILEM TC 119-TCE, TCE1: Adiabatic and semi-adiabatic calorimetry to determine the temperature increase in concrete due to hydration heat of the cement, *Mat. Struct.* 30 (8) (1997) 451–464, <https://doi.org/10.1007/BF02524773>.
- [46] EN 1015-6, Methods of test for mortar for masonry - Part 6: Determination of bulk density of fresh mortar, European Committee for Standardization, Brussels (Belgium), 1990.
- [47] EN 1015-10, Methods of test for mortar for masonry - Part 10: Determination of dry bulk density of hardened mortar, European Committee for Standardization, Brussels (Belgium), 1999.
- [48] ASTM C109/C109M-16a, Standard Test Method for Compressive Strength of Hydraulic Cement Mortars (Using 2-in. or [50 mm] Cube Specimens), ASTM International, West Conshohocken (PA, USA), 2016. [https://doi.org/10.1520/C0109\\_C0109M-20B](https://doi.org/10.1520/C0109_C0109M-20B).
- [49] ACI 229R-13, Report on Controlled Low Strength Materials, American Concrete Institute, Farmington Hill (MI, USA), 2013.
- [50] T.M. Do, Y.S. Kim, Engineering properties of controlled low strength material (CLSM) incorporating red mud, *Int. J. Geo-Eng.* 7 (7) (2016) 17, <https://doi.org/10.1186/s40703-016-0022-y>.
- [51] T.M. Do, H.K. Kim, M.J. Kim, Y.S. Kim, Utilization of controlled low strength material (CLSM) as a novel grout for geothermal systems: Laboratory and field experiments, *J. Build. Eng.* 29 (2020) 101110, <https://doi.org/10.1016/j.jobe.2019.101110>.
- [52] ASTM C940–16, Standard Test Method for Expansion and Bleeding of Freshly Mixed Grouts for Preplaced-Aggregate Concrete in the Laboratory, ASTM International, West Conshohocken (PA, USA), 2016. <https://doi.org/10.1520/C0940-16>.
- [53] G. Lombardi, The role of cohesion in cement grouting of rock, in: Proceedings of the 15th International Congress on Large Dams – ICOLD, Lausanne (Switzerland), Q.58 R.13, 1985, pp. 235–261.
- [54] M.R. Azadi, A. Taghichian, A. Taheri, Optimization of cement-based grouts using chemical additives, *J. Rock Mech. Geotech. Eng.* 9 (4) (2017) 623–637, <https://doi.org/10.1016/j.jrmge.2016.11.013>.
- [55] Y. Popov, G. Beardsmore, C. Clauser, S. Roy, ISRM suggested methods for determining thermal properties of rocks from laboratory tests at atmospheric pressure, *Rock. Mech. Rock. Eng.* 49 (10) (2016) 4179–4207, <https://doi.org/10.1007/s00603-016-1070-5>.
- [56] EN 1936, Natural stone test methods - Determination of real density and apparent density, and of total and open porosity, European Committee for Standardization, Brussels (Belgium), 2006.
- [57] D.V. Oliveira, R.A. Silva, E. Garbin, P.B. Lourenço, Strengthening of three-leaf stone masonry walls: an experimental research, *Mater. Struct.* 45 (8) (2012) 1259–1276, <https://doi.org/10.1617/s11527-012-9832-3>.
- [58] V. Alizadeh, A Rapid Construction Technique for Bridge Abutments Using Controlled Low Strength Materials (CLSM), The University of Wisconsin-Milwaukee Milwaukee (Wisconsin, USA), Ph.D. Thesis Dissertation. <https://dc.uwm.edu/etd/556>, 2013 (accessed 21 March 2019).
- [59] EN 445, Grout for Prestressing Tendons - Test Methods, European Committee for Standardization, Brussels (Belgium), 2007.
- [60] R. Le Roy, N. Roussel, The marsh cone as a viscometer: Theoretical analysis and practical limits, *Mat. Struct.* 38 (1) (2005) 25–30, <https://doi.org/10.1007/BF02480571>.
- [61] N. Roussel, R. Le Roy, The Marsh cone: a test or a rheological apparatus? *Cement. Concrete. Res.* 35 (5) (2005) 823–830, <https://doi.org/10.1016/j.cemconres.2004.08.019>.
- [62] ASTM C939/C939M-16a, Standard Test Method for Flow of Grout for Preplaced-Aggregate Concrete (Flow Cone Method), ASTM International, West Conshohocken (PA, USA), 2016. [https://doi.org/10.1520/C0939\\_C0939M-16A](https://doi.org/10.1520/C0939_C0939M-16A).
- [63] F. De Larrard, C. Ferraris, T. Sedran, Fresh concrete: a Herschel-Bulkley material, *Mat. Struct.* 31 (7) (1998) 494–498, <https://doi.org/10.1007/BF02480474>.
- [64] N. Roussel, *Understanding the Rheology Of Concrete*, Woodhead Publishing, Cambridge (UK), 2012.
- [65] R. Maglione, G. Robotti, R. Romagnoli, In-situ rheological characterization of drilling mud, *SPE J.* 5 (4) (2000) 377–386, <https://doi.org/10.2118/66285-PA>.
- [66] A.S. Georgiadis, K.K. Sideris, N.S. Anagnostopoulos, Properties of SCC produced with limestone filler or viscosity modifying admixture, *J. Mater. Civ. Eng.* 22 (4) (2010) 352–360, [https://doi.org/10.1061/\(asce\)mt.1943-5533.0000030](https://doi.org/10.1061/(asce)mt.1943-5533.0000030).
- [67] R.A. Schankoski, P.R. de Matos, R. Pilar, L.R. Prudêncio, R.D. Ferron, Rheological properties and surface finish quality of eco-friendly self-compacting concretes containing quarry waste powders, *J. Clean. Prod.* 257 (2020) 120508, <https://doi.org/10.1016/j.jclepro.2020.120508>.
- [68] Z. Rudzionis, E. Ivanauskas, M. Senkus, The analysis of secondary raw materials usage in self-compacting concrete production, *Mater. Sci.* 11 (3) (2005) 272–277.
- [69] A. Abdalqader, M. Sonebi, Dolomitic filler in self-compacting concrete: a review, *RILEM Tech. Lett.* 5 (2020) 75–83, <https://doi.org/10.21809/rilemtechlett.2020.118>.
- [70] D.R. Katti, L. Srinivasamurthy, K.S. Katti, Molecular modeling of initiation of interlayer swelling in Na–montmorillonite expansive clay, *Can. Geotech. J.* 52 (9) (2015) 1385–1395, <https://doi.org/10.1139/cgj-2014-0309>.
- [71] H.F.W. Taylor, *Cement Chemistry*, second ed., Thomas Telford, London (UK), 1997.
- [72] A.M. Neville, *Properties of Concrete*, forth ed., Prentice Hall, New York, 1995.
- [73] P. Monnot, Guide techniques et norms appliqués à la géothermie très basse énergie – Bilan de l'année 2013 – Rapport final BRGM/RP–63016–FR, Bureau de Recherches Géologiques et Minières, Orléans (France). <http://infoterre.brgm.fr/rapports/RP-63016-FR.pdf>, 2013 (last access 1 March 2021).
- [74] ASTM C191-19, Standard Test Methods for Time of Setting of Hydraulic Cement by Vicat Needle, ASTM International, West Conshohocken (PA, USA), 2019. <https://doi.org/10.1520/C0191-19>.
- [75] ASTM C403/C403M–16, Standard Test Method for Time of Setting of Concrete Mixtures by Penetration Resistance, ASTM International, West Conshohocken (PA, USA), 2016. [https://doi.org/10.1520/C0403\\_C0403M-16](https://doi.org/10.1520/C0403_C0403M-16).
- [76] X. Kang, H. Lei, Z. Xia, A comparative study of modified fall cone method and semi-adiabatic calorimetry for measurement of setting time of cement based materials, *Constr. Build. Mater.* 248 (2020) 118634, <https://doi.org/10.1016/j.conbuildmat.2020.118634>.
- [77] C. Zhang, J. Yang, X. Ou, J. Fu, Y. Xie, X. Liang, Clay dosage and water/cement ratio of clay-cement grout for optimal engineering performance, *Appl. Clay. Sci.* 163 (2018) 312–318, <https://doi.org/10.1016/j.clay.2018.07.035>.
- [78] T.M. Do, G.O. Kang, G.H. Go, Y.S. Kim, Evaluation of coal ash-based CLSM made with cementless binder as a thermal grout for borehole heat exchangers, *J. Mater. Civ. Eng.* 31 (6) (2018) 04019072, [https://doi.org/10.1061/\(ASCE\)MT.1943-5533.0002691](https://doi.org/10.1061/(ASCE)MT.1943-5533.0002691).
- [79] F. de Larrard, *Concrete Mixture Proportioning*, E&FN Spon, London (UK), 1999.
- [80] A.M. Neville, J.J. Brooks, *Concrete Technology*, second ed., Prentice Hall, New York, 2010.
- [81] S.A. Jefferis, The grouting of prestressing ducts, in: P.L.J. Domone, S.A. Jefferis (Eds.), *Structural Grouts*, Blackie Academic & Professional, London (UK), 1994, pp. 194–216.
- [82] EN 447, Grout for prestressing tendons - Basic requirements, European Committee for Standardization, Brussels (Belgium), 2007.
- [83] VDI 4640-2, Thermal use of the Underground - Ground Source Heat Pump Systems, Verein Deutscher Ingenieure e.V., Düsseldorf (Germany), 2019.
- [84] K.S. Chang, M.J. Kim, Thermal performance evaluation of vertical U-loop ground heat exchanger using in-situ thermal response test, *Renew. Energ.* 87 (2016) 585–591, <https://doi.org/10.1016/j.renene.2015.10.059>.
- [85] M. Allan, A. Philippopoulos, Performance characteristics and modelling of cementitious grouts for geothermal heat pumps, in: Proceedings of the World Geothermal Congress, Kyushu–Tohoku (Japan), 2000, pp. 3355–3360. <https://www.geothermal-energy.org/pdf/IGAstandard/WGC/2000/R0095.PDF>, (last access 1 March 2021).
- [86] L. Alberti, A. Angelotti, M. Antelmi, I. La Licata, A numerical study on the impact of grouting material on borehole heat exchangers performance in aquifers, *Energies* 10 (5) (2017) 703, <https://doi.org/10.3390/en10050703>.
- [87] L. Zhang, Q. Zhang, G. Huang, X. Ma, Transient ground and grout parameters estimation method for a ground-coupled heat pump system with sandbox TRT reference data, *Procedia Engineer.* 205 (2017) 2662–2669, <https://doi.org/10.1016/j.proeng.2017.10.217>.
- [88] F. Bozzoli, G. Pagliarini, S. Rainieri, L. Schiavi, Estimation of soil and grout thermal properties through a TSPEP (two-step parameter estimation procedure) applied to TRT (thermal response test) data, *Energy* 36 (2) (2011) 839–846, <https://doi.org/10.1016/j.energy.2010.12.031>.
- [89] A. Priarone, M. Fossa, Transient thermal resistance of borehole heat exchangers for hourly simulations of geothermal heat pumps systems, in: Proceedings of the IGSHPA Technical/Research Conference and Expo 2017, International Ground Source Heat Pump Association, 2017, p. 9. <https://doi.org/10.22488/okstate.17.000544>.
- [90] E. Di Sipio, D. Bertermann, Factors influencing the thermal efficiency of horizontal ground heat exchangers, *Energies* 10 (11) (2017) 1897, <https://doi.org/10.3390/en10111897>.
- [91] E. Di Sipio, D. Bertermann, Soil thermal behavior in different moisture condition: an overview of ITER Project from laboratory to field test monitoring, *Environ. Earth. Sci.* 77 (2018) 283, <https://doi.org/10.1007/s12665-018-7454-y>.
- [92] Y. Dong, J.S. McCartney, N. Lu, Critical review of thermal conductivity models for unsaturated soils, *Geotech. Geol. Eng.* 33 (2) (2015) 207–221, <https://doi.org/10.1007/s10706-015-9843-2>.

- [93] T.S. Yun, J.C. Santamarina, Fundamental study of thermal conduction in dry soils, *Granul. Matter.* 10 (3) (2008) 197–207, <https://doi.org/10.1007/s10035-007-0051-5>.
- [94] API Task Group on Cements for Geothermal Wells, API work group reports field tests of geothermal cements, *Oil and Gas Jour.* 11 (1985) 93–97.
- [95] M. Kruszewski, M. Glissner, S. Hahn, V. Wittig, Alkali-activated aluminosilicate sealing system for deep high-temperature well applications, *Geothermics* 89 (2021) 101935, <https://doi.org/10.1016/j.geothermics.2020.101935>.
- [96] M.R. Valluzzi, Comportamento meccanico di murature consolidate con materiali e tecniche a base di calce, Ph.D. Thesis Dissertation (in Italian), University of Trieste, Trieste (Italy). <https://www.openstarts.units.it/handle/10077/11393>, 2000 (accessed 3 June 2019).
- [97] M. Milan, Cantierabilità di iniezioni consolidanti con miscele non cementizie – applicazione al museo archeologico di Verona, M.Sc. Thesis Dissertation (in Italian), University of Padova, Padova (Italy). <http://tesi.cab.unipd.it/48924/>, 2015 (accessed 3 June 2019).
- [98] G. Gustafson, H. Stille, Prediction of groutability from grout properties and hydrogeological data, *Tunn. Undergr. Sp. Tech.* 11 (3) (1996) 325–332, [https://doi.org/10.1016/0886-7798\(96\)00027-2](https://doi.org/10.1016/0886-7798(96)00027-2).
- [99] A.C. Houslsby. *Construction and Design Of Cement Grouting: A Guide to Grouting in Rock Foundations*, John Wiley & Sons Inc., New York (USA), 1990.
- [100] K. Khayat, A. Yahia, Simple field tests to characterize fluidity and washout resistance of structural cement grout, *Cement. Concrete Aggr.* 20 (1) (1998) 145–156.
- [101] H. Vikan, S. Jacobsen, Influence of rheology on the pumpability of mortar. COIN report TG 2.1 Sintef, Trondheim (Norway) (2010). <http://hdl.handle.net/11250/2386793> (Accessed 1 March 2020).
- [102] M.H. Mohammed, R. Pusch, S. Knutsson, G. Hellström, Rheological Properties of Cement-Based Grouts Determined by Different Techniques, *Engineering* 6 (5) (2014) 217–229, <https://doi.org/10.4236/eng.2014.65026>.
- [103] F. Jorne, F.M.A. Henriques, L.G. Baltazar, Injection capacity of hydraulic lime grouts in different porous media, *Mater. Struct.* 48 (7) (2015) 2211–2233, <https://doi.org/10.1617/s11527-014-0304-9>.
- [104] E.Y. Gökyiğit-Arpaci, D. Oktay, N. Yüzer, S. Ulukaya, D. Ekşi-Akbulut, Performance evaluation of lime-based grout used for consolidation of brick masonry walls, *J. Mater. Civ. Eng.* 31 (6) (2019) 04019059, [https://doi.org/10.1061/\(ASCE\)MT.1943-5533.0002692](https://doi.org/10.1061/(ASCE)MT.1943-5533.0002692).
- [105] B. Dinç-Şengönül, D. Oktay, N. Yüzer, Effect of temperature, resting time and brick dust (Horasan) on the rheological properties of hydraulic lime-based grouts, *Constr. Build. Mater.* 265 (2020) 120644, <https://doi.org/10.1016/j.conbuildmat.2020.120644>.